EurJIC
European Journal of Inorganic Chemistry

A Journal of ChemPubSoc Europe

Accepted Article

Title: Mono- and bisruthenium, symmetrical and unsymmetrical complexes bridged by pyrene derivative - experimental and theoretical studies

Authors: Dawid Zych, Aneta Slodek, Michał Pająk, Stanisław Krompiec, Grzegorz Spólnik, and Witold Danikiewicz

To be cited as: *Eur. J. Inorg. Chem.* 10.1002/ejic.201700621

Link to VoR: http://dx.doi.org/10.1002/ejic.201700621

WILEY-VCH

10.1002/ejic.201700621

WILEY-VCH

Mono- and bisruthenium, symmetrical and unsymmetrical complexes bridged by pyrene derivative - experimental and theoretical studies

Dawid Zych*[a], Aneta Slodek[a], Michał Pająk[a], Stanisław Krompiec[a], Grzegorz Spólnik[b], Witold Danikiewicz[b]

Abstract: New mono- and bisruthenium, symmetrical and unsymmetrical complexes bridged by new cyclometalating 1,3,6,8-tetra(4-substituted-2-pyridyl)pyrene derivative containing solubilizing group - 2,2-dimethylpropyloxy with the terminal 4'-phenyl-2,2':6',2''-terpyridine ligands containing diethylamine and 2-ethynyl-9,9-dioctylfluorene moiety were synthesized and thoroughly characterized. Thermal studies showed that obtained complexes retain high thermal stability. Spectroscopic studies showed the metal-to-ligand-charge-transfer (MLCT) excitation. What is more, the electrochemical studies showed delocalization of the electronic charge (mixed-valance). In addition, density functional theory (DFT) and time-dependent-density functional theory (TD-DFT) calculations were performed to provide more details about structural properties and deeper understanding of the experimental results. All obtained results showed the considerable differences between mono- and bisruthenium and symmetrical and unsymmetrical complexes.

Introduction

Ruthenium complexes bridged by 1,3,6,8-tetrasubstituted pyrene, 2,3,5,6-tetrasubstituted pyrazine, and 1,2,4,5-tetrasubstituted benzene derivatives have been the subject of studies of a number of research groups for twenty years [1-4]. The interest of this kind of compounds is due to their appealing and unique electronic properties, such as wide electronic absorption spectra in the UV/Vis range, tunable potential energy and possible change between different oxidation states [5]. Moreover, ruthenium complexes have the ability to undergo metal-to-ligand-charge-transfer (MLCT) excitation and delocalization of the electronic charge (mixed-valance) [6]. What is more, they can be used in many applications, such as information storage [7], molecular wires [8], dynamic aircraft camouflage [9], electrochromic uses [10] and others. The wide range of interesting properties and potential applications is a reason that various ruthenium complexes have drawn great interest and new systems should be still developed.
Complexes of type $[(tpy)M(NCN\text{-}pyrene\text{-}NCN)M(tpy)]^{n+}$ where tpy is a terpyridine ligand, NCN-pyrene-NCN is a polydentate cyclometalating pyrene ligand and M is ruthenium metal have been investigated only by one research group. Yu-Wu Zhong, et al. began studies with cyclometalated mono- and bisruthenium complexes bridged by the simple derivative of pyrene, 1,3,6,8-tetra(2-pyridyl)pyrene [11]. The same research team showed the other bridging ligand 1,3,6,8-tetrakis(1-butyl-1H-1,2,3-triazol-4-yl)pyrene [12]. Using this kind of ligands as a core of complex do not provide good solubility, what is important in further research for the application. It was found that electronic properties of the mentioned above complexes are strongly dependent on the substituents in terminal ligands and their nature (electron-donating and electron-withdrawing groups) [13]. The influence of the changing of substituents in the bridge pyrene ligand has been relatively unexplored, only two were checked. Binuclear complexes of ruthenium are comprehensively experimentally as well as theoretically studied while the monoruthenium complexes need to be more investigated. What is more, all described in the literature binuclear complexes containing pyrene as a bridge are symmetrical.
In this study, we present the synthesis with efficient way of purification of novel mono- **(3)Ru(TPY1)** (**A1**) and bisruthenium, symmetrical (**TPY1)Ru(3)Ru(TPY1)** (**A2**), (**TPY2)Ru(3)Ru(TPY2)** (**A3**) and unsymmetrical (**TPY1)Ru(3)Ru(TPY2)** (**A4**) complexes bridged by new 1,3,6,8-tetra(4-substituted-2-pyridyl)pyrene derivative (**3**) containing solubilizing group i.e. 2,2-dimethylpropyloxy. The terminal ligands contain electron-rich substituents, namely N,N-diethylamine (**TPY1**) and 2-ethynyl-9,9-dioctylfluorene (**TPY2**), in the *para* position of the phenyl ring of terpyridine. The ligands **TPY1** and **TPY2** were intentionally chosen to examine their effect on optical and electronic properties of the formed complexes. These substituents have emerged to examine the influence of replacement fluorene group by diethylamine unit possessing stronger electron-donating ability on photophysical properties of the desired complexes **A1**–**A4**, including absorption, band gaps, HOMO and LUMO. On the other hand, the presence of acetylene linker in **TPY2** can affect the geometry of resulting complexes and cause better delocalization of the excited electron on the ligand connected with the conjugated unit which better stabilizes the LUMO orbital [14].
Moreover, spectroscopic, electrochemical and theoretical studies have been investigated in details.

Results and Discussion

Synthesis and structural characterization

The synthesis of the bridge i.e. 1,3,6,8-tetra(4-(2,2-dimethylpropyloxy)-2-pyridyl)pyrene **3** is presented in Scheme 1. The first step was based on well-known reaction bromination of commercially available pyrene, what resulted in 1,3,6,8-tetrabromopyrene **1** in 98% yield [15]. The Suzuki-Miyaura coupling reaction between **1** and bis(pinacolato)diboron with catalyst $[Pd(pddf)_2Cl_2]$ afforded to 1,3,6,8-tetrakis(4,4,5,5-tetramethyl-1,3,2-dioxaborolan-2-yl)pyrene **2** in 75% yield [16]. The target derivative **3** was synthesized in Suzuki-Miyaura Pd-catalyzed cross-coupling reaction between tetrasubstituted boronic acid pyrene derivative **2** and 4-(2,2-dimethylpropyloxy)pyridine what resulted in the product as a yellow solid in 62% yield (for a detailed description of synthesis see Supporting Information).

[a] Institute of Chemistry, Faculty of Mathematics, Physics and Chemistry, University of Silesia, Szkolna 9, 40-007 Katowice, Poland
E-mail: dawidzych92@gmail.com
[b] Institute of Organic Chemistry, Polish Academy of Sciences, Kasprzaka 44/52, 01-224 Warszawa 42, Poland

Supporting information for this article is given via a link at the end of the document.

10.1002/ejic.201700621

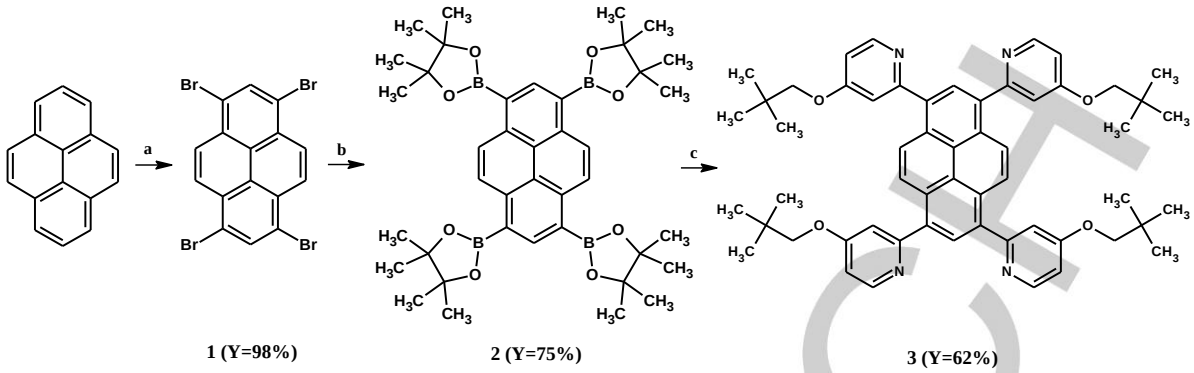

Scheme 1. Synthesis route to tetrasubstituted pyrene intermediates **1**, **2** and **3**. *Reagents and reaction conditions:* **a)** Br_2, $PhNO_2$, reflux, 16 h; **b)** bis(pinacolato)diboron, KOAc, [$PdCl_2$(dppf)], PhMe, 90 ºC, 24 h; **c)** 2-bromo-4-(2,2-dimethylpropyloxy)pyridine, K_3PO_4*$3H_2O$, [$Pd(PPh_3)_4$], DME/H_2O, 105 ºC, 48 h.

Scheme 2 shows the synthesis routes to terpyridine ligands **TPY1** and **TPY2**. First step was conducted based on described in the literature procedure from commercially available appropriate 4-substituted benzaldehyde and 2-acetylpyridine in Kröhnke reaction and resulted in **TPY1** as a green solid in 34% yield or 4'-(4-bromophenyl)-2,2':6',2''-terpyridine **4**, respectively, whereas **4** was used in the next step [17]. The Sonogashira cross-coupling reaction of **4** with trimethylsilylacetylene (TMSA) catalyzed by [$Pd(PPh_3)_4$] gave 4'-(4-ethynylphenyl)-2,2':6',2''-terpyridine **5** in 92% yield which was reacted with 2-iodo-9,9-dioctylfluorene by using [Pd]/[Cu]-catalyzed Sonogashira cross-coupling reaction what resulted in **TPY2** as a dark yellow oil in 60% yield [18,19].

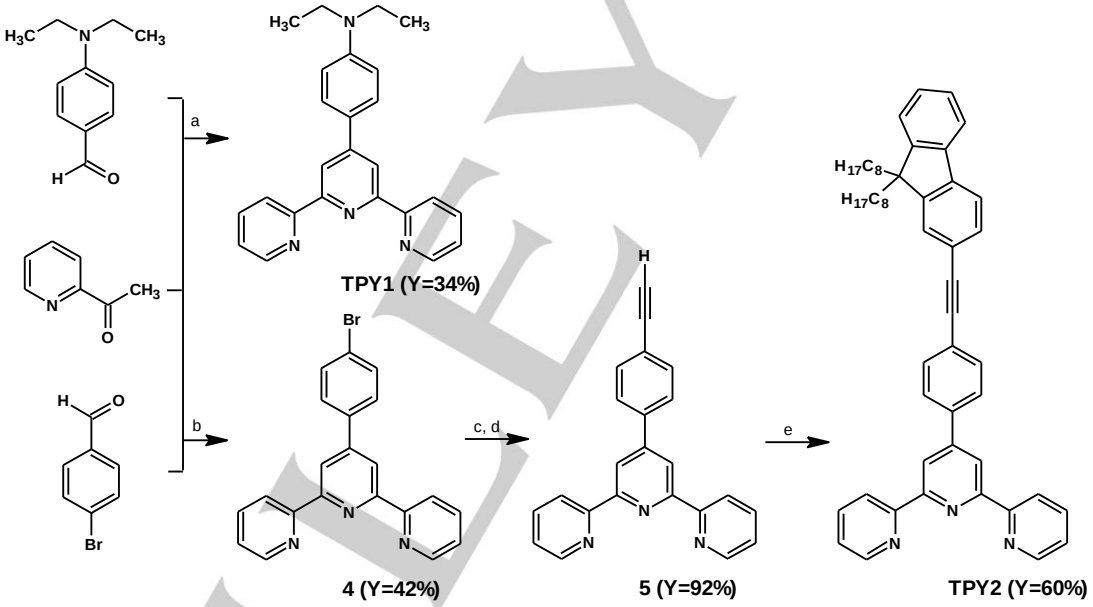

Scheme 2. Synthesis of compounds **TPY1**, **TPY2** and **4**, **5**. *Reagents and conditions*: **a)** KOH, $NH_{3\ aq}$, EtOH, reflux, 16 h; **b)** KOH, $NH_{3\ aq}$, EtOH, room temp., 24 h; **c)** TMSA, [$Pd(PPh_3)_4$], CuI, NEt_3, reflux, 16 h; **d**) KF, THF, MeOH, room temp., 24 h; **e)** 2-iodo-9,9-dioctylfluorene, [$Pd(PPh_3)_4$], CuI, THF, NEt_3, 78 ºC, 48 h.

Ruthenium complexes with appropriate terpyridine ligand (TPY)$RuCl_3$ were synthesized in satisfactory yields according to the well-known procedure [20] and used without any purification in reaction with silver triflate (AgOTf) what resulted in a product with labile triflate group [21]. Obtained in this way intermediate was reacted with neutral pyrene ligand **3** (Scheme 3). The final complexes **A1**–**A3** were precipitated by addition of $KPF_{6(aq)}$. Sequential column chromatography (silica gel chromatography followed by size-exclusion chromatography) was required to isolate the pure product. Respective proportions of reactants allowed to obtain monoruthenium **A1** in 56% yield and bisruthenium **A2** (48%) and **A3** (50%) complexes as black solids. Moreover, the unsymmetrical bisruthenium complex **A4** was obtained based on the same procedure described above with minor modification; monoruthenium complex **A1** was added instead of neutral pyrene ligand (Scheme 4). The product **A4** was obtained in 17% yield as a black solid.

All compounds were fully characterized by nuclear magnetic resonance spectroscopy NMR (^{1}H for **A1**–**A4** and ^{13}C for **A1**), high-resolution mass spectrometry (HRMS), and elemental analysis. The experimental isotopic patterns compared with theoretical for **A1** and **A2** are depicted in Figure 1, for more details see Experimental section and Supporting Information (Figure S6-S14).

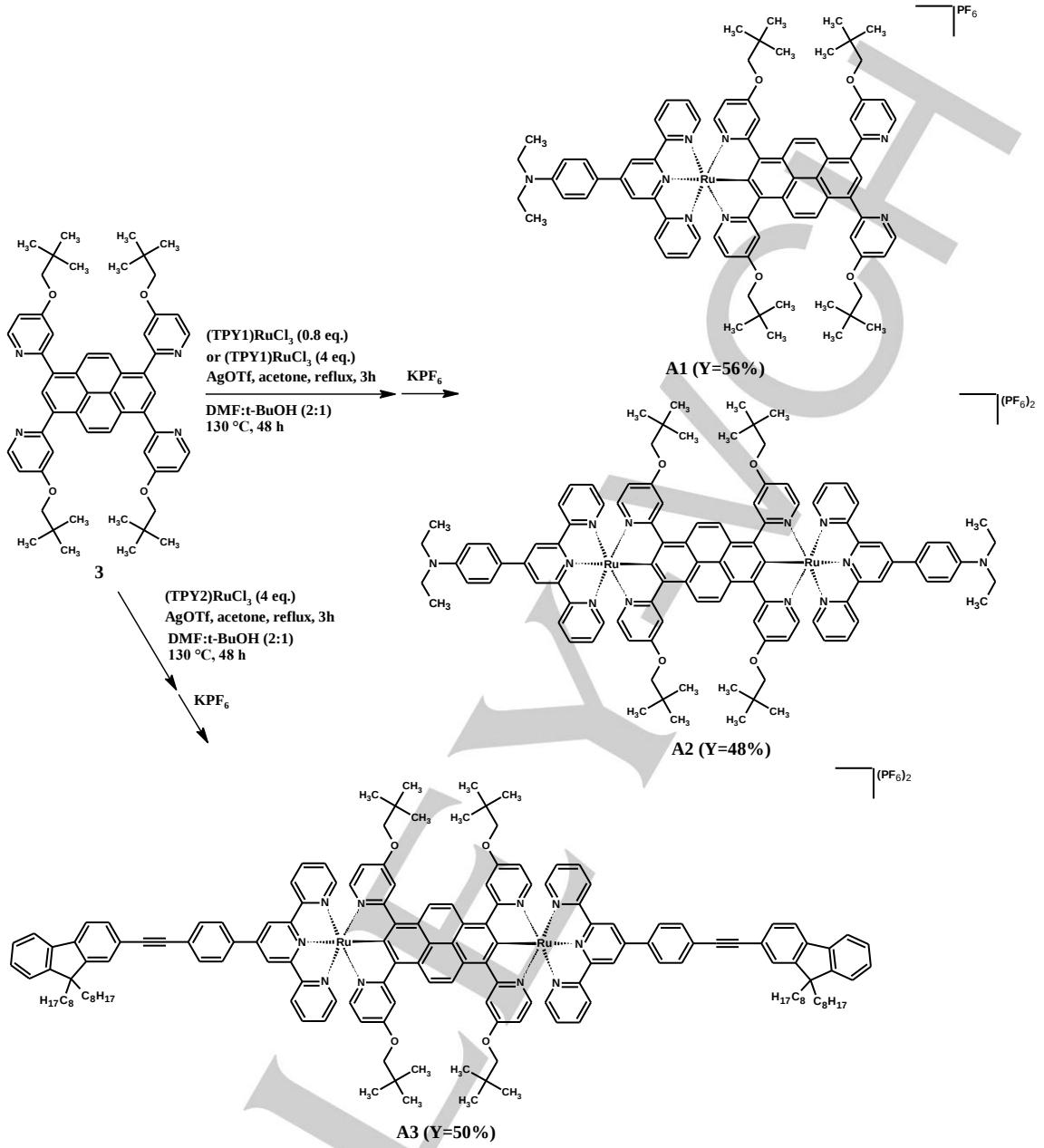

Scheme 3. Synthesis of designed complexes **A1**, **A2,** and **A3**.

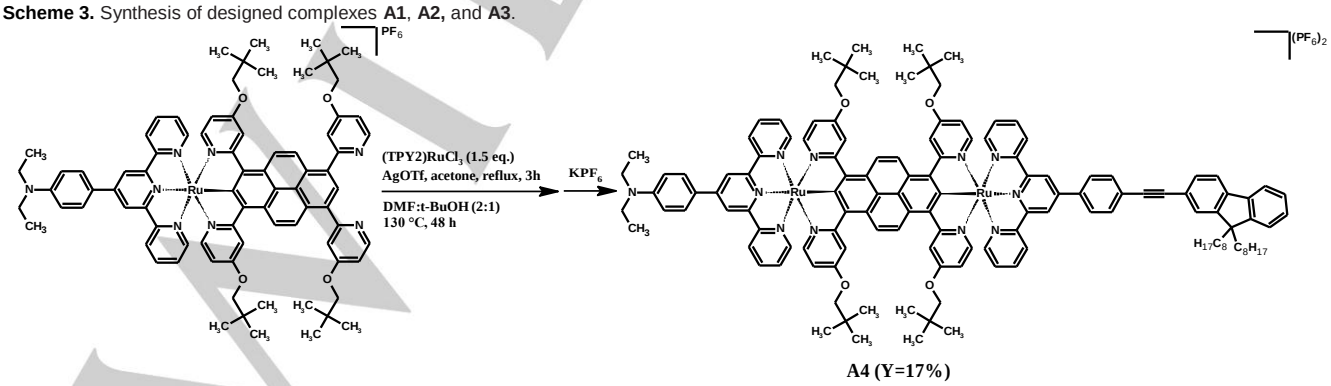

Scheme 4. Synthesis of the designed unsymmetrical complex **A4**.

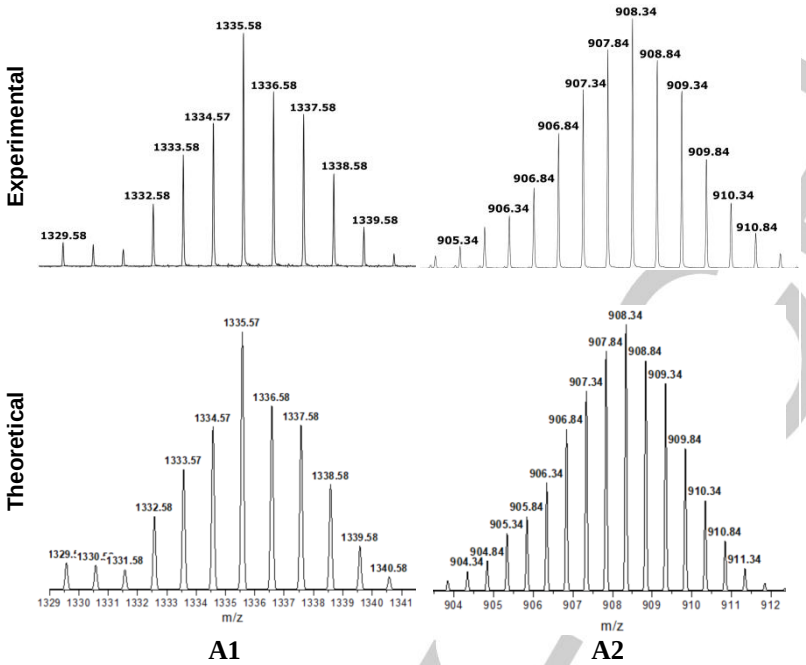

Figure 1. Theoretical and experimental isotopic patterns for **A1** and **A2**.

Thermal properties

The thermal properties of the investigated compounds **A1**–**A4** were examined by differential scanning calorimetry (DSC) and thermogravimetric analysis (TGA) under a nitrogen atmosphere; the obtained results are shown in Table 1, whereas Figure 2 presents representative TGA and DTG thermograms for mononuclear **A1** and binuclear unsymmetrical **A4** complexes. The TGA results showed that molecules retain high thermal stability. Decomposition temperature corresponding to 5% weight loss ($T_{5\%}$) for mononuclear complex **A1** is higher in comparison to binuclear complexes **A2**–**A4** and exalts 299 °C. The temperature of 5% decomposition for **A2**–**A4** is in the range of 198 - 233 °C whereas the temperature of unsymmetrical binuclear complex **A4** is located between the temperatures of symmetrical complexes **A2** and **A3** built from the same terminal ligands. The char residue observed at 900 °C is the highest for monoruthenium complex **A1** and then for **A4**. Symmetrical complexes **A2** and **A3** generated similar percent of residue. DSC investigations for all compounds did not show any transitions in the range of -145 °C – 195 °C.

Table 1. Thermal properties of the synthesized derivatives **A1**–**A4**.

Code	TGA			
	$T_{5\%}$ [°C]	$T_{10\%}$ [°C]	T_{max} [°C]	Char residue at 900 °C [%]
A1	299	378	425, 705	54
A2	198	282	220, 416, 499, 716	15
A3	233	278	272, 431, 496	17
A4	202	268	209, 286, 429, 713	41

$T_{5\%}$, $T_{10\%}$ – temperature of 5% and 10% weight loss, respectively; T_{max} - the maximum decomposition rate from DTG thermograms

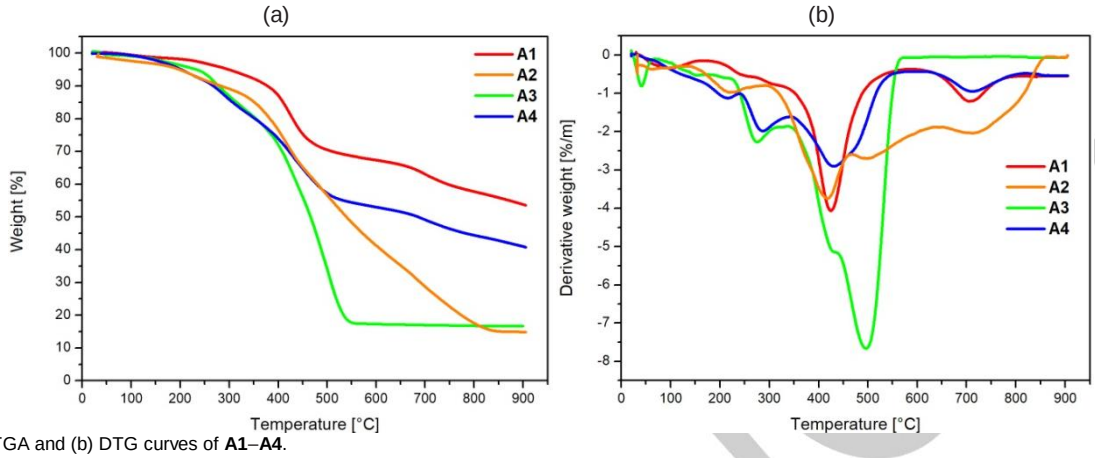

Figure 2. (a) TGA and (b) DTG curves of **A1**–**A4**.

Theoretical studies

In order to gain the information about the geometry and optical properties of the mono- and bisruthenium complexes **A1**–**A4** density functional theory (DFT) and time-dependent-density functional theory (TD-DFT) calculations were performed by using Gaussian 09 program [22]. The B3LYP exchange-correlation functional with Def2-TZVP basis set for ruthenium and 6-31G(d) for others atoms was employed. All calculations were carried out in CH_3CN as a solvent in the polarisable continuous model (PCM). The B3LYP/Def2-TZVP; 6-31G(d) optimized structures for **A1**–**A4** are presented in Supporting Information as Figure S1. In the presented structures terminal ligands are in a perpendicular plane to the bridging ligand. The substituents in terpyridines are not coplanar in relation to the central pyridine ring. The bonds length between ruthenium and carbon in presented complexes are showed in Table 2, the length of Ru-C for monoruthenium complex **A1** is the shortest.

Electrostatic potential energy maps for **A1**–**A4** are showed in Figure S2 in Supporting Information, they illustrate the charge distributions of molecules three-dimensionally. It can determinate how molecules interact with others.

What is more, representation of the frontier molecular orbitals (HOMOs and LUMOs) and energy gap (ΔE) for described compounds were also calculated. The obtained results are listed in Table 2. The value of ΔE for **A1**–**A4** is respectively 2.61 eV, 2.22 eV, 2.26 eV and 2.24 eV. The energy gap for monoruthenium complex **A1** is the highest whereas the difference between HOMO and LUMO for bisruthenium unsymmetrical complex **A4** is between the energy of symmetrical binuclear complexes **A2** and **A3** which are built from the same terminal ligands.

Table 2. Calculated frontier orbitals HOMO and LUMO, energy gap and bond length Ru-C for **A1**-**A4**.

	A1	**A2**	**A3**	**A4**
HOMO [eV]	-5.01	-4.83	-4.90	-4.87
LUMO [eV]	-2.40	-2.61	-2.64	-2.63
ΔE [eV]	2.61	2.22	2.26	2.24
Ru-C [Å]	1.985	1.987	1.989	1.986/1.989

The frontier orbitals for **A1**–**A4** are presented in Figure 3. In the case of monoruthenium complex **A1**, the electrons in the Highest Occupied Molecular Orbital (HOMO) are mainly localized on terpyridine ligand and ruthenium atom but the Lowest Unoccupied Molecular Orbital (LUMO) is delocalized on pyrene ligand. Separation of frontier orbitals for monoruthenium complex was achieved. In the case of bisruthenium complex **A4**, the HOMO and LUMO are localized on the core of the molecule, bridging ligand, the part of the occupied frontier orbital is also localized on the ruthenium metal. The same distribution of frontier orbitals is for binuclear, symmetrical complexes **A2** and **A3**. The pyridines in the bridging pyrene ligand in mono- and bisruthenium complexes take a slight part in the creation of frontier orbitals whereas alkoxy chains do not participate at all. The same results of theoretical studies for binuclear, symmetrical complexes are described by Yu-Wu Zhong, et al. [13]. The contours of other selected orbitals for **A1** and **A4** are depicted in Figure S3 and S4 in Supporting Information.

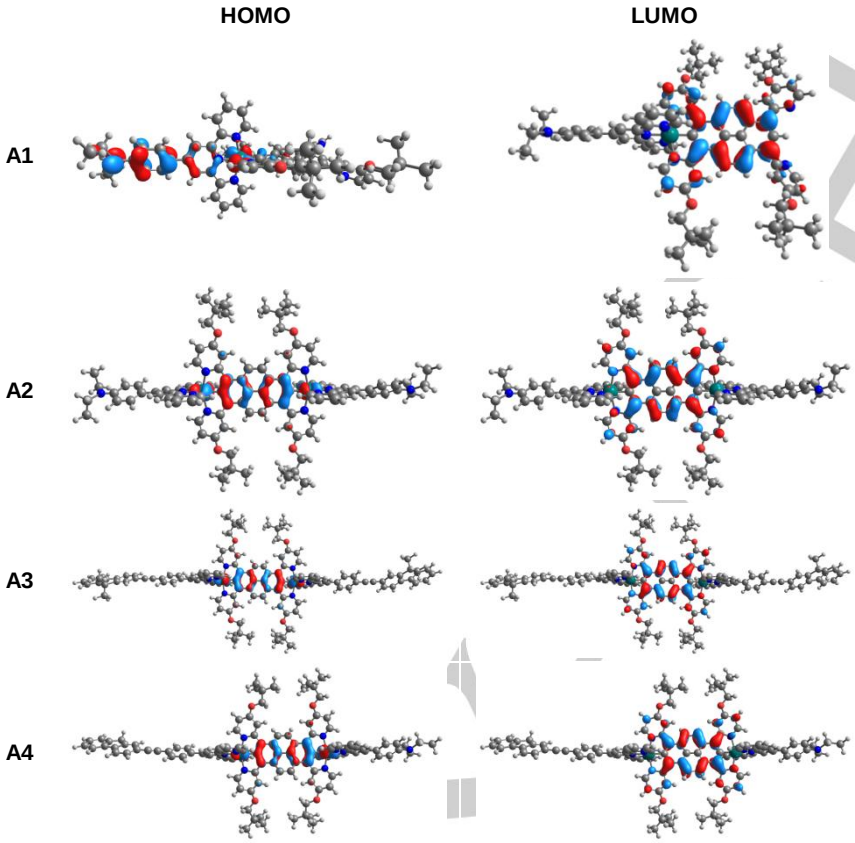

Figure 3. The HOMOs and LUMOs of **A1**-**A4**.

Moreover, the time-dependent-density functional theory calculations were performed for compounds **A1**–**A4**. The obtained results are discussed in the part concerning optical properties and TD-DFT study.

Optical properties and TD-DFT study

The UV/Vis spectra of the new complexes **A1**–**A4** were investigated in acetonitrile (CH_3CN) solutions at room temperature. The obtained results are presented in Figure 6. The absorption maxima and molar extinction data are shown in Table 3. The assignment of bands is discussed based on the results from theoretical studies (TD-DFT calculations) which were also carried out using the same level of theory as DFT study.

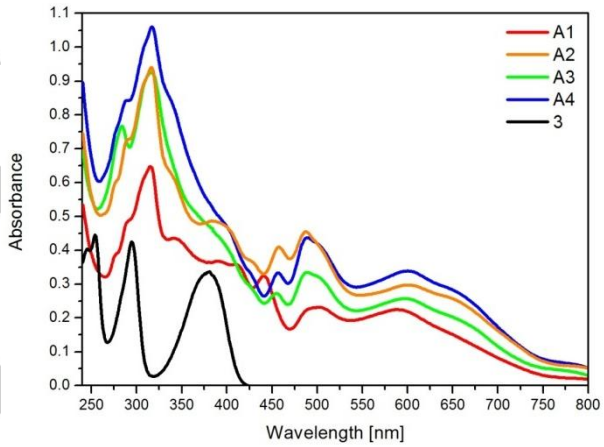

Figure 6. The UV/Vis spectra of complexes **A1**–**A4** and NCN-coordinating pyrene ligand **3** in acetonitrile solution ($c = 10^{-5}$ mol/L).

Table 3. Absorption data for **A1**–**A4** and **3**.

Code	λ_{max}/nm (ε/10^5 M^{-1} cm^{-1})
A1	593 (0.22), 502 (0.23), 441 (0.33), 409 (0.36), 391 (0.37), 343 (0.44), 316 (0.65), 290 (0.49), 277^{sh} (0.39)
A2	652^{sh} (0.26), 602 (0.30), 488 (0.46), 458 (0.41), 427 (0.37), 384 (0.49), 339^{sh} (0.63), 317 (0.94), 289^{sh} (0.72), 277^{sh} (0.60)
A3	657^{sh} (0.20), 601 (0.26), 490 (0.33), 455 (0.27), 396^{sh} (0.42), 316 (0.93), 284 (0.77)
A4	651^{sh} (0.28), 602 (0.34), 489 (0.44), 457 (0.33), 404^{sh} (0.45), 338^{sh} (0.85), 317 (1.06), 289 (0.84)
3	381 (0.34), 295 (0.43), 254 (0.45)

^{sh} - shoulder

The predicted electronic transitions for **A1** and **A4** compared with experimental spectra are shown in Figure 7 and for **A2** and **A3** in Supporting Information (Figure S5). The calculated wavelength in absorption spectra, oscillator frequencies (f) and character of dominant transitions are listed in Table S1-S4 in Supporting Information.

In general, predicted excitations are in accordance with the experimental data with differences up to 50 nm what can be related to solvent polarity and explained by specific solvent effects. What is more, the difference may be caused by a large π-conjugated system of examined compounds **A1**–**A4**. In the range of spectra, the same number of main bands was seen.

For all complexes absorption bands in UV region between 240 and 427 nm are connected with intraligand transitions π→π* from NCN-coordinating pyrene ligand **3** and terminal terpyridine ligands. In Vis region four for bisruthenium complexes **A2**–**A4** and three for mononuclear complex **A1** main absorption bands are seen. The intensity of monoruthenium complex **A1** in comparison to bisruthenium complexes **A2**–**A4** is even one and a half less. It is worth mention that similar phenomenon is observed for monoruthenium and bisruthenium complexes with 1,3,6,8-tetra(2-pyridyl)pyrene as bridging ligand [11].

The absorption band with the lowest energy for **A2**–**A4** are shown as a shoulder.

In the case of monoruthenium complex **A1**, the band at 593 nm is associated with H-1→LUMO and HOMO→LUMO transitions (593.8 nm, f=0.0612). It is the mixed character of metal-to-ligand-charge-transfer (MLCT) transitions from ruthenium to pyrene and charge transfer from terpyridine to pyrene ligand. The rest bands can be interpreted as intraligand transitions as well as transitions between terpyridine and pyrene ligands, whereas excitations at 391 nm (379.6 nm, f=0.1185; HOMO→L+3) and 343 nm (334.4 nm, f=0.3969; HOMO→L+8) have also the partial character of MLCT transition. In unsymmetrical bisruthenium complex **A4**, the band at 651 nm is associated with HOMO→LUMO transitions (697.3 nm, f=0.1179) what correspond to mix of MLCT from ruthenium to pyrene and intraligand charge transfer of pyrene. The other bands can be described as intraligand transitions and transitions between various part of molecule i.e. TPY1→TPY2, pyrene→TPY. The trend of predicted excitations of bisruthenium complexes **A2**–**A4** show that they have similar assignments for their absorption bands.

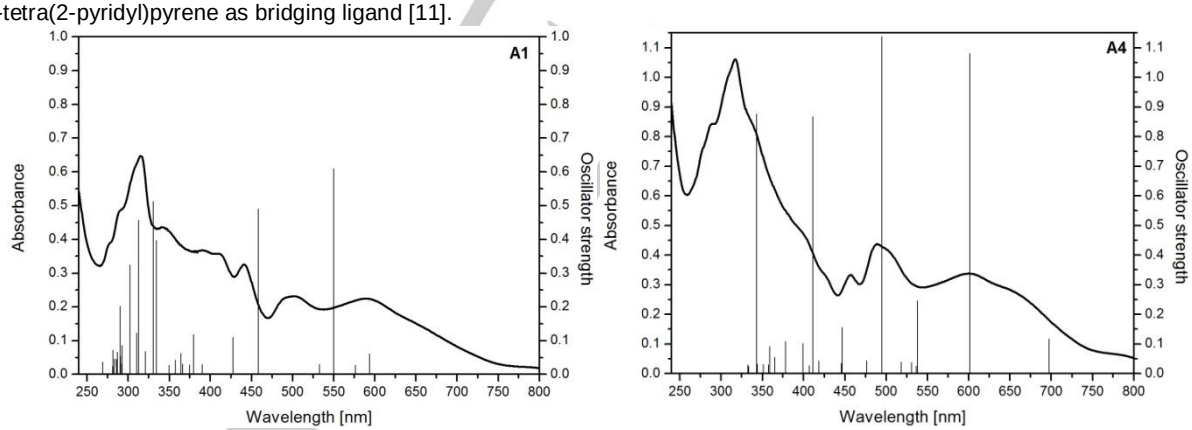

Figure 7. UV/Vis spectra in CH3CN and TD-DFT predicted excitations (B3LYP/Def2-TZVP; 6-31G(d)/CH3CN) for **A1** and **A4**.

Electrochemical Properties

The electrochemical behavior of ruthenium complexes **A1**–**A4** in N,N-dimethylformamide (DMF) solution was examined by cyclic voltammetry (CV) and differential pulse voltammetry (DPV). The obtained electrochemical data are presented in Table 5 and 6.

The electrochemical oxidation and reduction onset potentials were used to estimate ionization potentials (IP) and electron affinities of the materials (it was assumed that the IP of ferrocene (Fc) equals -5.1 eV) [23]. The calculated ionization potentials values, electron affinities together with the electrochemical band gaps energy (E_g) are presented in Table 5 and Table 6. For all of the examined compounds, the reduction peaks were recorded in the potential range from -2.11 to -1.21 V It is worth noting that for all of the examined complexes multi-step reduction was observed. All the observed reduction processes are fully reversible. It can be noted that all the reduction processes occur on pyrene and terpyridine ligands. The reduction processes of bisruthenium unsymmetrical complex **A4** occur harder (at about 100 mV lower potential) than the same reduction processes of symmetrical complex **A3** but slightly easier than monoruthenium complex **A1** with diethylamine substituent at the terpyridine. It is probably related to electron donating character of amine moiety in the terpyridine ligand.

For all of the examined compounds **A1**–**A4** the oxidation peaks were recorded at a potential range between -0.07 and 0.52 V. Undoubtedly, the first oxidation occurs at the ruthenium atoms, which corresponds well with the literature [3]. All the observed oxidation processes are fully reversible. It is worth noting that the first oxidation peak of **A1** is recorded between two oxidation peaks of **A2** (Table 6). It may be that the delocalization of electrons along the pyrene ligand is more favored in the mixed-valence states than in the homovalent ones. It is the common electrochemical behavior of those complexes [24].

The electrochemical band gaps ($E_{g\ el}$) for examined compounds vary from 1.29 to 1.54 eV which corresponds well with the band gaps calculated from UV/Vis spectra (1.62 eV for **A1** and 1.53 eV for **A2**–**A3**).

Table 5. Electrochemical data for **A1**–**A4** recorded in DMF solution.

	$E_{ox(CV)}$[V]	$E_{ox(DPV)}$[V]	$E_{red(CV)}$[V]	$E_{red(DPV)}$[V]	HOMO [eV][1]	LUMO [eV][2]	$E_{g\ el}$ [eV][3]	$E_{g\ opt}$ [eV][4]	$E_{g\ (DFT)}$ [eV]
A1	0.08	-0.05	-1.46	-1.43	-5.18	-3.64	1.54	1.62	2.61
A2	0.04	-0.08	-1.36	-1.27	-5.14	-3.74	1.40	1.53	2.22
A3	0.09	0.04	-1.21	-1.29	-5.19	-3.89	1.30	1.53	2.26
A4	-0.07	-0.17	-1.36	-1.42	-5.03	-3.74	1.29	1.53	2.24

[1]E_{HOMO}= - 5.1 - $E_{ox,\ onset}$; [2]E_{LUMO}= - 5.1 - $E_{red,\ onset}$; [3]$E_{g\ el}$ = $E_{ox,\ onset}$ - $E_{red,\ onset}$ = E_{HOMO} - E_{LUMO}
[4]calc. from: Eg=1240/λ_{abs}

Table 6. Comparison of peak onsets (CV) for **A1**–**A4** recorded in DMF solution.

	E_{red1}[V]	E_{red2}[V]	E_{red3}[V]	E_{red4}[V]	E_{ox1}[V]	E_{ox2}[V]	E_{ox3}[V]
A1	-1.46	-1.67	-1.93	-2.11	0.08	0.23	-
A2	-1.36	-1.65	-1.72	-	0.04	0.19	-
A3	-1.21	-1.45	-1.73	-	0.09	0.29	-
A4	-1.36	-1.56	-1.86	-	-0.07	0.17	0.52

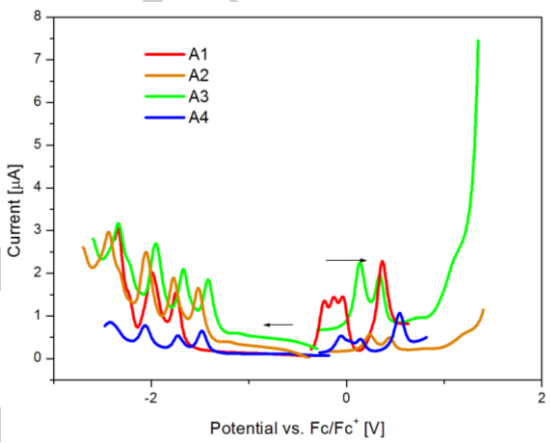

Figure 8. DPV scans for **A1**–**A4** in DMF with 0.1 M Bu_4NPF_6; sweep rate *v* = 10 mV/s. The measurements were performed with a glassy carbon working electrode and referenced against the Fc/Fc^+ couple. The arrows show the scan direction.

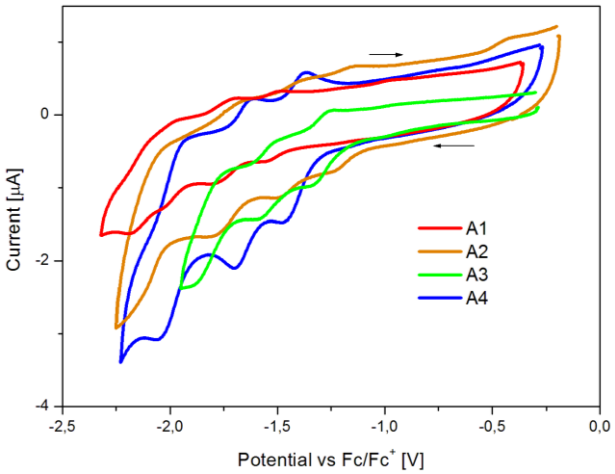

Figure 9. Cyclic voltammograms recorded during the reduction of **A1**–**A4** in DMF. The measurements were performed with a glassy carbon working electrode and referenced against the Fc/Fc$^+$ couple; sweep rate *v*= 100 mV/s. The arrows show the scan direction.

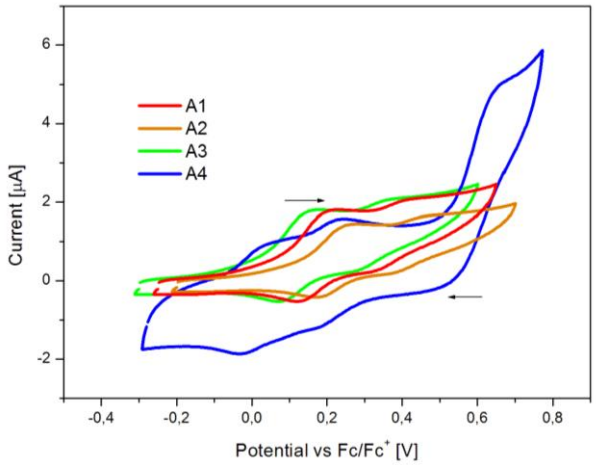

Figure 10. Cyclic voltammograms recorded during the oxidation of **A1**–**A4** in DMF. The measurements were performed with a glassy carbon working electrode and referenced against the Fc/Fc$^+$ couple; sweep rate *v* =100 mV/s. The arrows show the scan direction.

Conclusions

We presented the synthesis with efficient way of purification and comprehensive characterization of novel mono- (**A1**) and bisruthenium, symmetrical (**A2** and **A3**) and unsymmetrical (**A4**) complexes bridged by new 1,3,6,8-tetra(4-substituted-2-pyridyl)pyrene derivative containing solubilizing group 2,2-dimethylpropyloxy with the terminal 4'-phenyl-2,2':6',2''-terpyridine ligands containing amine and 2-ethynyl-9,9-dioctylfluorene moiety. The described molecules **A1**–**A4** were prepared with moderate yields in the range of 17-56%. All reported in this article compounds are soluble and thermally stable. The presented experimental, as well as theoretical studies, showed the considerable differences between mono- and bisruthenium complexes whereas the difference between symmetrical and unsymmetrical complexes are definitely less significant. The absorption spectra are consistent in comparison with results obtained from TD-DFT studies. What is more, the electrochemical investigation showed that the first oxidation peak of monoruthenium complex **A1** is recorded between two oxidation peaks of bisruthenium **A2**. It showed delocalization of the electronic charge (mixed-valance). This kind of complex may be of interest for a further test for the application. Monoruthenium complexes in comparison to bisruthenium complexes shown the meaningful differences what was proofed in presented work.

Experimental Section

Materials

All chemicals and starting materials were commercially available and were used without further purification. Solvents were distilled as per the standard methods and purged with nitrogen before use. All reactions were carried out under argon atmosphere unless otherwise indicated. Column chromatography was carried out on Merck silica gel. Size-exclusion chromatography was carried out on Sephadex LH-20 GE Healthcare. Thin layer chromatography (TLC) was performed on silica gel (MerckTLCSilicaGel60).

General Procedure for the synthesis of mono- and bisruthenium complexes A1–A3: To 50 mL of acetone appropriate (TPY)$RuCl_3$ (0.024 mmol for **A1**; 0.12 mmol for **A2** and **A3**) and AgOTf (0.08 mmol for **A1**; 0.40 mmol for **A2** and **A3**) were added and the mixture was stirring at 65 °C for 3 h. After cooling to room temperature the mixture was filtered through Celite and the filtrate was evaporated. The obtained residue, 1,3,6,8-tetrakis(4-(2,2-dimethylpropyloxy)-2-pyridyl)pyrene (0.026 g, 0.03

mmol), t-BuOH (8 mL) and DMF (8 mL) were placed in 20 mL vial and capped. The mixture was saturated with argon, heated to 130 ºC and stirred for 48 h. After cooling to a room temperature aqua solution of KPF_6 (10 mL) was added and resulting precipitate was collected by vacuum filtration and washed with water. The crude product was purified by column chromatography (silica gel; $CH_3CN:H_2O:KPF_{6(aq)}$ (100:1:2)) followed by size-exclusion chromatography on Sephadex LH-20 (CH_3CN:MeOH (2:1)). The trailing edge of the product band contained small traces of other species was discarded. Fractions with the pure product were evaporated to dryness.

Procedure for the synthesis of unsymmetrical bisruthenium complex A4: To 25 mL of acetone **(TPY2)RuCl$_3$** (0.023 g, 0.025 mmol) and AgOTf (0.025 g, 0.1 mmol) were added and the mixture was stirring at 65 °C for 3 h. After cooling to room temperature the mixture was filtered through Celite and the filtrate was evaporated. Obtained residue, monoruthenium complex **A1** (0.033 g, 0.023 mmol), t-BuOH (5 mL) and DMF (5 mL) were placed in 20 mL vial and capped. The mixture was saturated with argon, heated to 130 ºC and stirred for 48 h. After cooling to a room temperature aqua solution of KPF_6 (10 mL) was added and resulting precipitate was collected by vacuum filtration and washed with water. The crude product was purified by column chromatography (silica gel; $CH_3CN:H_2O:KPF_{6(aq)}$ (100:1:2)) followed by size-exclusion chromatography on Sephadex LH-20 (CH_3CN:MeOH (2:1)). Fractions with the pure product were evaporated to dryness.

A1 (20 mg, 56%) as black solid
^{1}H NMR (400 MHz, Acetone) δ 9.26 (s, *J* = 12.5 Hz, 2H), 9.11 (d, *J* = 9.5 Hz, 2H), 8.87 (d, *J* = 8.2 Hz, 2H), 8.75 (d, *J* = 9.4 Hz, 2H), 8.36 (d, *J* = 2.7 Hz, 2H), 8.30 (s, 1H), 8.21 (d, *J* = 8.7 Hz, 2H), 7.80 (t, *J* = 7.8 Hz, 2H), 7.56 (d, *J* = 1.8 Hz, 2H), 7.29 (t, *J* = 7.3 Hz, 2H), 7.23 (d, *J* = 6.4 Hz, 2H), 7.20 – 7.13 (m, 2H), 7.08 – 6.98 (m, 6H), 6.50 (dd, *J* = 6.5, 2.9 Hz, 2H), 3.97 (s, 4H), 3.81 (s, 4H), 3.66 – 3.54 (m, 4H), 1.28 (s, *J* = 10.1, 6.9 Hz, 6H), 1.11 (s, 18H), 1.00 (s, 18H).
^{13}C NMR (101 MHz, Acetone) δ 170.79, 167.01, 166.02, 161.85, 160.39, 155.52, 154.01, 153.26, 151.63, 149.89, 145.60, 137.93, 136.80, 135.54, 129.34, 129.01, 128.58, 128.50, 128.03, 128.00, 127.13, 124.34, 124.32, 123.91, 118.90, 113.17, 112.91, 111.63, 110.00, 109.31, 78.66, 78.56, 68.03, 44.99, 32.41, 32.30, 26.74, 26.61.
HRMS (ESI): *m/z* calcd. for $C_{81}H_{85}N_8O_4Ru$ $[M]^+$ 1335.5737; found 1335.5769.
Anal. Cald. for $C_{81}H_{85}F_6N_8O_4PRu$: C, 65.71; H, 5.79; N, 7.57. Found: C, 65.50; H, 5.93; N, 7.41.

A2 (30 mg, 48%) as black solid
^{1}H NMR (400 MHz, Acetone) δ 9.37 (d, *J* = 17.9 Hz, 4H), 9.32 – 9.24 (m, 2H), 8.91 (d, *J* = 8.1 Hz, 6H), 8.52 (t, *J* = 7.8 Hz, 2H), 8.26 (d, *J* = 8.5 Hz, 8H), 7.91 (dd, *J* = 16.0, 9.1 Hz, 8H), 7.29 – 7.15 (m, 8H), 7.04 (d, *J* = 8.5 Hz, 6H), 7.00 – 6.90 (m, 2H), 6.61 – 6.36 (m, 4H), 3.91 (s, 8H), 3.61 (dd, *J* = 14.0, 6.8 Hz, 14H), 1.05 (s, 36H).
HRMS (ESI): *m/z* calcd. for $C_{106}H_{108}N_{12}O_4Ru_2$ $[M]^{2+}$ 908.3352; found 908.3400.
Anal. Cald. for $C_{106}H_{108}F_{12}N_{12}O_4P_2Ru_2$: C, 60.45; H, 5.17; N, 7.98. Found: C, 60.55; H, 5.26; N, 7.86.

A3 (42 mg, 50%) as black solid
^{1}H NMR (400 MHz, Acetone) δ 9.40 (s, *J* = 7.3 Hz, 4H), 9.36 (d, *J* = 10.6 Hz, 4H), 8.93 (d, *J* = 8.1 Hz, 4H), 8.50 (s, 4H), 8.26 (d, *J* = 7.9 Hz, 4H), 7.88 – 7.72 (m, 8H), 7.59 (d, *J* = 8.0 Hz, 4H), 7.43 – 7.34 (m, 6H), 7.34 – 7.24 (m, 4H), 7.17 (d, *J* = 6.5 Hz, 4H), 7.11 – 7.05 (m, 4H), 6.90 (d, *J* = 5.5 Hz, 2H), 6.81 (d, *J* = 12.1 Hz, 2H), 6.50 (d, *J* = 7.2 Hz, 4H), 3.85 (s, 8H), 1.35 (t, *J* = 4.8 Hz, 8H), 1.22 (s, 12H), 1.08 – 0.98 (m, 72H), 0.68 – 0.59 (m, 12H).
HRMS (ESI): *m/z* calcd. for $C_{160}H_{174}N_{10}O_4Ru_2$ $[M+4H]^{2+}$ 1251.5904; found 1251.5953.
Anal. Cald. for $C_{160}H_{170}F_{12}N_{10}O_4P_2Ru_2$: C, 68.90; H, 6.14; N, 5.02. Found: C, 68.99; H, 6.30; N, 4.98.

A4 (10 mg, 17%) as black solid
^{1}H NMR (400 MHz, Acetone) δ 9.51 (s, 1H), 9.45 – 9.40 (m, 4H), 9.32 (s, 2H), 9.03 (d, *J* = 8.0 Hz, 2H), 8.95 (d, *J* = 8.0 Hz, 2H), 8.56 (dd, *J* = 4.4, 2.5 Hz, 4H), 8.50 (d, *J* = 8.5 Hz, 1H), 8.26 (d, *J* = 8.8 Hz, 2H), 7.96 – 7.80 (m, 8H), 7.73 (s, 1H), 7.65 (dd, *J* = 8.1, 5.5 Hz, 2H), 7.54 – 7.50 (m, 1H), 7.44 (dd, *J* = 7.3, 4.8 Hz, 2H), 7.38 (dt, *J* = 7.3, 2.4 Hz, 4H), 7.29 (ddd, *J* = 9.1, 6.6, 3.2 Hz, 4H), 7.21 (dd, *J* = 7.2, 3.4 Hz, 1H), 7.14 (dd, *J* = 13.6, 6.3 Hz, 2H), 7.09 (dd, *J* = 10.1, 4.2 Hz, 1H), 7.04 (t, *J* = 6.1 Hz, 2H), 6.59 (ddd, *J* = 8.8, 6.4, 2.4 Hz, 4H), 3.91 (s, 8H), 3.61 (dd, *J* = 14.1, 7.0 Hz, 4H), 1.42 – 1.38 (m, 6H), 1.35 – 1.26 (m, 14H), 1.14 – 1.09 (m, 8H), 1.09 – 1.04 (m, 36H), 0.91 – 0.78 (m, 8H), 0.74 – 0.61 (m, 4H).
HRMS (ESI): *m/z* calcd. for $C_{133}H_{140}N_{11}O_4Ru_2$ $[M+H]^{2+}$ 1079.4589; found 1079.4600.
Anal. Cald. for $C_{133}H_{139}F_{12}N_{11}O_4P_2Ru_2$: C, 65.26; H, 5.72; N, 6.30. Found: C, 65.41; H, 5.77; N, 6.19.

Measurements: NMR spectra were recorded in CD_3COCD_3 with Bruker Advance 400 MHz instruments (for ^{1}H and ^{13}C NMR).
High-resolution mass spectrometry (HRMS) measurements were performed using Synapt G2-S mass spectrometer (Waters) equipped with the electrospray ion source and quadrupole-Time-of-flight mass analyzer. Methanol was used as a solvent with the flow rate 100 µl/min. The measurement was performed in positive ion mode with the capillary voltage set to 3 kV. The desolvation gas flow was 400 L/h and temperature 150 °C. The sampling cone was set to 20 V and the source temperature was 120 °C. To ensure accurate mass measurements, data were collected in centroid mode and mass was corrected during acquisition using leucine enkephalin solution as an external reference (Lock-SprayTM), which generated reference ion at *m/z* 556.2771 Da ($[M + H]^+$) in positive ESI mode. The results of the measurements were processed using the MassLynx 4.1 software (Waters) incorporated with the instrument.
Elemental analysis was performed by using Perkin Elmer Series II CHNS/O Analyzer 2400 in CHN operating mode. The sample before the measurement was dried for 6 h under vacuum (0,2 mbar, 60°C).
Differential Scanning Calorimetry (DSC) was measured with a TA-DSC 2010 apparatus, under a nitrogen atmosphere with heating/cooling rate 20 deg/min. Thermogravimetric analysis (TGA) was done using TGA/DSC1 Mettler-Toledo thermal analyzer with a heating rate of 10 ºC/min in a stream of nitrogen (60 cm^3/min^1).

Spectroscopic Measurements: UV/Vis spectra were recorded by using Perkin–Elmer Lambda Bio 40 UV/Vis spectrophotometer at room temperature in denoted solvents with a conventional 1.0 cm quartz cell.

Electrochemical Measurements: Electrochemical measurements were carried out using Eco Chemie Autolab PGSTAT128n potentiostat, glassy carbon electrode (diam. 2 mm), platinum coil and silver wire as working, auxiliary and a reference electrode, respectively. Potentials are referenced with respect to ferrocene (Fc), which was used as the internal standard. Cyclic voltammetry experiments were conducted in a standard one-compartment cell, in DMF (Carlo Erba, HPLC grade), under argon. 0.2M Bu_4NPF_6 (Aldrich, 99%) was used as the supporting electrolyte. The concentration of compounds was equal $1.0 \cdot 10^{-6}$ mol/dm^3. Deaeration of the solution was achieved by argon bubbling through the solution for about 10 min before measurement. All electrochemical experiments were carried out under ambient conditions.

Acknowledgements

This work was supported by the Ministry of Science and Higher Education, Poland (Diamentowy Grant number 0215/DIA/2015/44).
Calculations have been carried out using resources provided by Wroclaw Centre for Networking and Supercomputing (http://wcss.pl), grant No.18.

Keywords: Ru(II) complexes • Terpyridines • Electrochemistry • Theoretical study • Absorption spectra

[1] C.J. Yao, J. Yao, Y.W. Zhong, *Inorg. Chem.* **2012**, *51*, 6259-6263.
[2] T. Nagashima, T. Nakabayashi, T. Suzuki, K. Kanaizuka, H. Ozawa, Y.W. Zhong, S. Masaoka, K. Sakai, M. Haga, *Organometallics* **2014**, *33*, 4893-4904.
[3] R.R. Ruminski, T.D. Aasen, *Inorg. Chim. Acta* **2010**, *363*, 905-910.

[4] L.M. Vogler, S.W. Jones, G.E. Jensen, R.G. Brewer, K.J. Brewer, *Inorg. Chim. Acta*, **1996**, *250*, 155-162.
[5] J.A. McCleverty, T.J. Meyer, *Comprehensive Coordination Chemistry*, Elsevier, **2003**.
[6] T. Akasaka, T. Mutai, J. Otsuki, K. Araki, ***Dalton Trans.*** **2003**, 1537-1544.
[7] B.B. Cui, Z.P. Mao, Y.X. Chen, Y.W. Zhong, G. Yu, C. Zhan, J. Yao, *Chem. Sci*. **2015**, *6*, 1308-1315.
[8] H.M. Wen, Y. Yang, X.S. Zhou, J.Y. Liu, D.B. Zhang, Z.B. Chen, J.Y. Wang, Z.N. Chen, Z.Q. Tian, *Chem. Sci.* **2013**, *4*, 2471-2477.
[9] R.J. Mortimer, *Chem. Soc. Rev*. **1997**, 26, 147.
[10] C.J. Yao, Y.W. Zhong, H.J. Nie, H.D. Abruna, J. Yao, *J Am Chem Soc,* **2011**, 133, 20720–20723.
[11] C.J. Yao, L.Z. Sui, H.Y. Xie, W.J. Xiao, Y.W Zhong, J. Yao, *Inorg. Chem.* **2010**, *49*, 8347-8350.
[12] L. Wang, W.W. Yang, R.H. Zheng, Q. Shi, Y.W. Zhong, J. Yao, *Inorg. Chem.* **2011**, *50*, 7074-7079.
[13] C.J. Yao, H.J. Nie, W.W. Yang, J. Yao, Y.W. Zhong, *Inorg. Chem.* **2015**, *54*, 4688-4698.
[14] J.A. Treadway, B. Loeb, R. Lopez, P.A. Anderson, F.R. Keene, T.J. Meyer, *Inorg. Chem.* **1996**, *35*, 2242-2246.
[15] S. Bernhardt, M. Kastler, V. Enkelmann, M. Baumgarten, K. Mullen, *Chem. Eur. J.* **2006**, *12*, 6117-6128.
[16] B.A.G Hammer, M. Baumgarten, K. Mullen, *Chem. Commun.* **2014**, *50*, 2034-2036.
[17] S. Tu, T. Li, F. Shi, F. Fang, S. Zhu, X. Wei, Z. Zong, *Chemistry Letters* **2005**, *34(5)*, 732-733.
[18] V. Grosshenny, F. M. Romero, R. Ziessel, *J. Org. Chem.* **1997**, *62(5)*, 1491-1500.
[19] D. Zych, A. Slodek, M. Matussek, M. Filapek, G. Szfarniec-Gorol, S. Maślanka, S. Krompiec, S. Kotowicz, E. Schab-Balcerzak, K. Smolarek, S. Maćkowski, M. Olejnik, W. Danikiewicz, *Dyes Pigm.* **2017**, *146,* 331-343.
[20] B. P. Sullivan, J. M. Calvert, T. J. Meyer, *Inorg. Chem*. **1980**, *19*, 1404.
[21] V. Duprez, J.P. Launay, A. Gourdon, *Inorg. Chim. Acta*, **2003**, *343*, 395.
[22] M.J. Frisch, G.W. Trucks, H.B. Schlegel, G.E. Scuseria, M.A. Robb, J.R. Cheeseman, et.al. GAUSSIAN 09 (Revision B.01), Gaussian, Inc. Wallingford, CT; **2010**.
[23] P. Bujak, I. Kulszewicz-Bajer, M. Zagorska, V. Maurel, I. Wielgus, A. Pron, *Chem Soc Rev*. **2013**, *42*, 8895-8999.
[24] N. Chanda, B. Sarkar, S. Kar, J. Fiedler, Wolfgang Kaim,G.K. Lahiri, *Inorg. Chem.* **2004**, *43*, 5128−5133.

10.1002/ejic.201700621

FULL PAPER

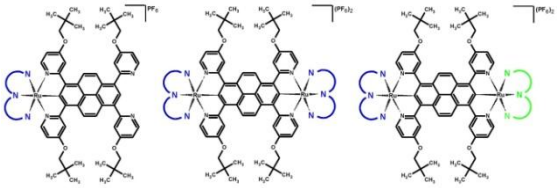

- Novel complexes bridged by pyrene derivative
- New cyclometalating 1,3,6,8-tetra(4-substituted-2-pyridyl)pyrene derivative containing solubilizing group - 2,2-dimethylpropyloxy
- Differences between mono- and bisruthenium, symmetrical and unsymmetrical complexes

Mono- and bisruthenium complexes

Dawid Zych, Aneta Slodek, Michał Pająk, Stanisław Krompiec, Grzegorz Spólnik, Witold Danikiewicz*

Page No. – Page No.

Mono- and bisruthenium, symmetrical and unsymmetrical complexes bridged by pyrene derivative - experimental and theoretical studies